Higher-Order Phase-Coupling Typicality for Detecting and Classifying Stealthy False Data Injection Attacks in Smart Grids

Mete Kağan Işıklı
Gazi University
Department of Electrical and Electronics Engineering
Ankara, Türkiye
23180202783@gazi.edu.tr

Seyfettin Vadi
Gazi University
Department of Electrical and Electronics Engineering
Ankara, Türkiye
seyfettinvadi@gazi.edu.tr

***Abstract*—Stealthy false data injection attacks (FDIAs), constructed as $a = Hc$, are invisible to the classical bad-data detector (BDD) by preserving the measurement residual. This paper investigates higher-order phase structure as an alternative detection signal. Normal grid signals are expected to carry quadratic phase coupling (QPC) among harmonic components, a structure invisible to second-order statistics, and an FDIA which does not faithfully reproduce this coupling should perturb it detectably. The proposed detector projects measurements into a mode space via PCA, scores per-mode bicoherence against normal statistics, and accumulates temporal deviations through an IIR filter. On the IEEE 118-bus benchmark with stealth FDIAs and branch-outage faults, bicoherence with IIR accumulation achieves 80.5% 3-class accuracy (11 features) and a Normal/FDIA pairwise AUC of 0.99 [0.98,1.00], surpassing two competitive baselines. An ablation study isolates the phase-coupling contribution: amplitude-only features yield only 17.8% accuracy despite 1824 dimensions. A QPC-aware adaptive attacker reduces detection AUC from 0.99 to 0.71, yet fails to reach the chance level (0.50), indicating that the $a{=}Hc$ constraint and phase-coupling preservation are in tension. On real PMU field data, the phase-locking value variant with IIR accumulation attains AUC 0.93. The detector is reconstruction-free, lightweight (11 handcrafted features), and interpretable.**

***Index Terms*—false data injection attack, state estimation, higher-order statistics, bicoherence, phase coupling, anomaly detection, smart grid security**

I. Introduction

Modern power grids collect real-time measurements from phasor measurement units (PMUs) and remote terminal units (RTUs) and transmit them to a control center for state estimation. This cyber-physical coupling exposes the grid to false data injection attacks (FDIAs), in which an adversary manipulates measurement data to corrupt the estimated state [1]. The canonical stealth attack $a = Hc$, introduced by Liu et al. [1], lies in the column space of the measurement Jacobian H and therefore leaves the BDD residual unchanged by construction. Advanced measurement technologies make it increasingly feasible for an attacker to mimic legitimate data while evading residual-based defenses.

A large body of data-driven FDIA detectors [2] flags anomalies through a reconstruction or prediction error learned from normal data. However, these detectors share the same structural vulnerability: an attacker who keeps the corrupted measurements close to the learned manifold can suppress the reconstruction error much as the stealth attack suppresses the BDD residual. The deeper question is whether there exists a signal that BDD and second-order detectors cannot see, yet a stealth FDIA unavoidably perturbs. This work investigates the answer through the lens of higher-order phase structure.

Our hypothesis is that normal grid signals carry quadratic phase coupling (QPC) among harmonic components, and that this coupling, invisible to the power spectrum and autocorrelation [3], is disrupted by FDIAs that do not faithfully reproduce the underlying phase relationships. The bicoherence, a normalized third-order statistic, quantifies this coupling strength [4]. A recent comprehensive survey cataloging over forty FDIA methods [2] lists no approach employing bicoherence, bispectrum, or phase-coupling statistics. The contributions of this work are:

1) A reconstruction-free, mode-space bicoherence detector augmented with an IIR temporal accumulation filter, requiring only 11 handcrafted features.
2) A controlled ablation study on the IEEE 118-bus benchmark comparing phase-blind amplitude features (17.8%, 1824D) against bicoherence with IIR accumulation (80.5%, 11D), isolating the independent contribution of phase-coupling information.
3) A QPC-aware adaptive attacker that reduces detection AUC from 0.99 to 0.71, providing empirical evidence of a structural constraint imposed by $a{=}Hc$.
4) An H-confounding check confirming that FDIA/Fault discrimination (AUC 0.97) reflects genuine physical differences rather than a projection artifact.

5) Validation on real PMU field data, where the PLV variant with IIR accumulation achieves AUC 0.93.

II. Related Work

FDIA Detection. Since Liu et al. [1] introduced the stealth FDIA, detection methods have employed residual-based tests, supervised classifiers, and reconstruction-based learning with autoencoders, graph neural networks, and transformers [2]. All of these ultimately score a reconstruction or prediction error. The work closest to ours is Tang et al. [5], who extended BDD detection to colored Gaussian noise via a generalized likelihood ratio test. However, their method remains a second-order statistic and does not exploit phase information. More recent approaches demonstrate that blind FDIAs constructed by learning the measurement manifold can evade reconstruction-based detectors [6], [7], motivating the search for complementary signals beyond the second order.

Higher-Order Spectral Analysis. The bispectrum and bicoherence were established by Nikias and Mendel [3] as tools for detecting quadratic phase coupling, with foundational digital implementations provided by Kim and Powers [4]. These methods have since been applied in biomedical signal processing (EEG), acoustics, plasma physics, and gravitational-wave detection. Within power systems, Chow and Gou [8] applied bispectral analysis to identify asymmetrical faults in induction machines; these methods target physical fault diagnosis, not FDIA detection. To the best of our knowledge, bicoherence has not previously been employed for FDIA detection in smart grids.

Fault vs. Attack Discrimination. Distinguishing cyber-attacks from physical faults is critical for timely response: misclassifying a fault as an attack delays corrective action, while the reverse risks unnecessary countermeasures. Most existing approaches rely on supervised deep learning with large labeled datasets [9]. Our method is unsupervised with respect to the attack type, requiring only normal-operation statistics, and uses 11 interpretable features.

III. Threat Model and Detection Mechanism

A. Stealth FDIA and BDD Blind Spot

The linear DC state estimation model is $z = Hx + e$, where $z \in \mathbb{R}^m$ is the measurement vector, $x \in \mathbb{R}^n$ the state vector, and $H \in \mathbb{R}^{m\times n}$ the Jacobian matrix encoding network topology. The BDD computes the residual $r = \|z - H\hat{x}\|_2$ and raises an alarm if r exceeds a threshold. A stealth FDIA injects an attack vector:

$$a = Hc \tag{1}$$

for an arbitrary $c \in \mathbb{R}^n$. This produces $z' = z + Hc = H(x + c) + e$, which preserves the residual exactly:

$$r' = \|P_\perp(z + Hc)\|_2 = \|P_\perp z\|_2 = r \tag{2}$$

where $P_\perp = I - H(H^TH)^{-1}H^T$ and $P_\perp H = 0$ by construction. (The unweighted least-squares form is presented for clarity; the stealth property holds identically for the weighted case, since Hc remains in $\mathrm{col}(H)$ regardless of the noise covariance.) The BDD is therefore structurally blind to any attack satisfying (1). Fig. 1 illustrates this geometry.

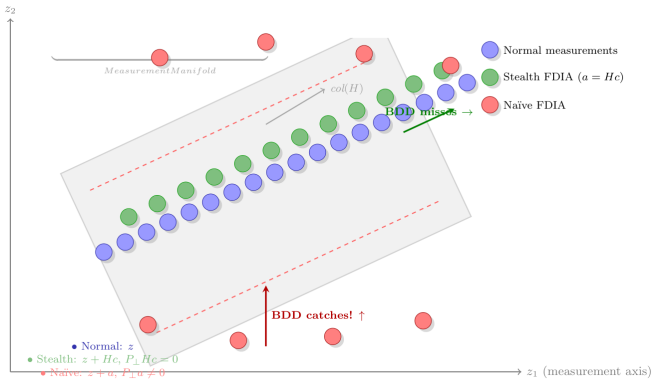

Fig. 1. Geometry of naïve vs. stealth FDIAs in measurement space. Normal measurements (blue) lie within the column space of H (gray band). Naïve attacks (red) deviate perpendicularly and are caught by the BDD (dashed lines). Stealth attacks $a = Hc$ (green) remain inside $\mathrm{col}(H)$ and are invisible to the BDD.

B. Quadratic Phase Coupling and Bicoherence

Real power system signals exhibit nonlinear dynamics that produce harmonic phase locking. A 24-hour load cycle generates harmonics at 12, 8, and 6 hours that remain phase-coupled to the fundamental because they share a common physical origin. Similarly, inter-area oscillations create phase-locked voltage fluctuations across multiple buses. This quadratic phase coupling (QPC) satisfies $\phi(f_1 + f_2) \approx \phi(f_1) + \phi(f_2)$ and is invisible to the power spectrum $|X(f)|^2$, which discards $\phi(f)$ entirely. The squared bicoherence quantifies QPC strength via segment-averaged triple products:

$$b^2(f_1, f_2) = \frac{\left|\frac{1}{S}\sum_s U_s(f_1)U_s(f_2)U_s^*(f_1 + f_2)\right|^2}{\frac{1}{S}\sum_s |U_s(f_1)U_s(f_2)|^2 \cdot \frac{1}{S}\sum_s |U_s(f_1 + f_2)|^2} \tag{3}$$

where $U_s(f)$ is the short-time Fourier transform of segment s and S is the number of independent segments. Segment averaging is essential: a single segment ($S = 1$) yields $b^2 \equiv 1$ trivially, regardless of whether genuine phase coupling exists. Only by averaging over independent realizations can true coupling (constant phase difference) be distinguished from random alignment (mean $\to 0$). Fig. 2 visualizes this: the locked signal exhibits a sharp bicoherence peak at (f_0, f_0), whereas the unlocked signal, sharing the identical power spectrum, shows near-zero bicoherence throughout.

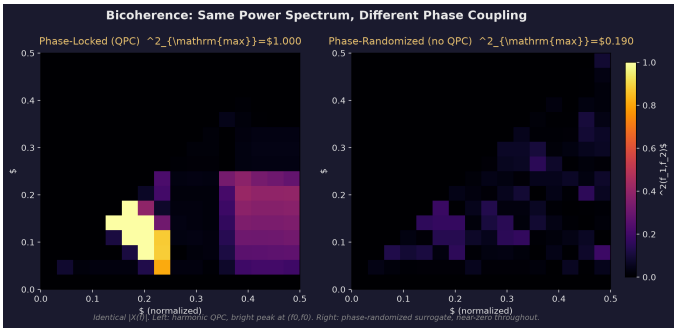

Fig. 2. Bicoherence heatmaps for a signal with (left) and without (right) quadratic phase coupling. Both signals have identical power spectra $|X(f)|^2$ and autocorrelation functions. Left: a bright peak at (f_0, f_0) confirms harmonic QPC ($b^2_{\max} \approx 1$). Right: phase-randomized surrogate with the same $|X(f)|$ shows no coupling ($b^2_{\max} \approx 0.19$).

C. Mode-Space Projection

Computing bicoherence directly on measurement channels proves ineffective: each channel is a linear mixture (through H) of modes with different fundamental frequencies, whose phase locks superpose destructively. Measurements are therefore projected into a mode space via PCA:

$$M = Q^\top H^+ Z \tag{4}$$

where H^+ is the Moore–Penrose pseudo-inverse, $Z \in \mathbb{R}^{N\times m\times W}$ contains N windows of W measurement samples, and $Q \in \mathbb{R}^{n\times K}$ comprises the top K principal components of normal operating states. Each mode signal $M_k \in \mathbb{R}^W$ is evaluated via (3) to yield a per-mode bicoherence vector $\mathbf{b}^2 \in [0,1]^K$.

D. IIR Cumulative Anomaly Score

A single-window bicoherence drop may originate from noise transients or brief oscillations rather than an attack. To capture sustained disruptions characteristic of FDIAs, deviations are accumulated over time using an exponential moving average:

$$S_t = \beta S_{t-1} + \left\|(\mathbf{b}_t^2 - \boldsymbol{\mu}_0) \oslash \boldsymbol{\sigma}_0\right\|_\infty \tag{5}$$

where $\boldsymbol{\mu}_0$ and $\boldsymbol{\sigma}_0$ are per-mode statistics from normal training windows, $\oslash$ denotes element-wise division, and $\beta \in [0,1)$ controls temporal memory. A sustained bicoherence drop (characteristic of FDIA) accumulates in S_t, while transient fluctuations (noise or brief faults) are attenuated by the exponential decay.

E. PLV Variant for PMU Data

PMU phasor data demodulates the fundamental grid frequency, removing the harmonic carrier needed for bicoherence. For such data, bicoherence is replaced with the phase-locking value (PLV) between PMU pairs, computed after band-pass filtering around the dominant oscillation mode:

$$\mathrm{PLV}_{ij} = \left|\frac{1}{T}\sum_{t=1}^{T} e^{j(\phi_i(t)-\phi_j(t))}\right| \tag{6}$$

where PLV ≈ 1 indicates stable inter-unit phase locking and PLV ≈ 0 indicates independent phases. The IIR score (5) is applied identically, with the per-mode bicoherence vector replaced by the per-pair PLV vector.

IV. Experimental Setup

A. Test Settings

The method is evaluated across three settings spanning increasing realism and decreasing experimental control (see Table I for detection results).

S1 – IEEE 118-Bus Synthetic: The Jacobian $H \in \mathbb{R}^{304\times 117}$ is obtained via the PyPower implementation of the MATPOWER [10] IEEE-118 test case. Normal states are generated from K=6 modes, each a fundamental frequency f_1 with a phase-locked second harmonic $2f_1$ ($\phi_2 = 2\phi_1$) and AR(1) temporal drift. Heteroscedastic AR-colored measurement noise is added. Window size W=256, 300 training + 250 test windows.

S2 – NYISO Hourly Load: 2024 hourly actual load data (11 zones, 8,205 h after removing incomplete records), detrended with a 168-hour moving average [11]. Sliding windows of W=192 h with 24 h step. Mode basis Q is obtained via PCA (K=6).

S3 – PMU Field Data: IEEE DataPort LFO dataset [12], 3 PMUs, 100 Hz sampling, 250 s duration, dominant oscillation at 0.854 Hz. Windows of W=1500 (15 s), 200-sample step. PLV replaces bicoherence.

TABLE I
Detection AUC across test settings (Bicoherence+IIR, attack strength α=2.0).

Setting	AUC [95% CI]	BDD AUC
S1 – IEEE-118	0.99 [0.98, 1.00]	0.50
S2 – NYISO	0.69 [0.61, 0.77]	0.50
S3 – PMU LFO	0.93 [0.89, 0.96]	—

B. Attack Models and Baselines

Stealth FDIA (naïve attacker): $a = Hc$ modulated by a phase-breaking harmonic (ϕ_1, ϕ_2 independent). This satisfies the stealth constraint (1) but does not reproduce the normal phase structure. Attack strength $\alpha \in \{0.5, 1, 2, 4\}$ scales c relative to the normal state standard deviation.

Physical Fault: A single random branch outage that alters the topology matrix H, genuinely changing the power flow.

Competitive Baselines: (A) BDD residual concatenated with per-channel amplitude statistics (mean, std, max, min, ptp, diff-std), fed to a Random Forest classifier (1825 features). (B) Isolation Forest on the BDD residual and measurement standard deviation (2 features).

Metrics: ROC-AUC for binary detection; 3-class accuracy for the Normal/FDIA/Fault discrimination task. All metrics are reported with bootstrap 95% confidence intervals (1,000 resamples).

V. Results

A. Mechanism Validation and Real-Data Evidence

It is verified that the detector scores phase structure rather than an energy shortcut through a locked-vs-unlocked control experiment. When normal data carries harmonic phase locking ($\phi_2 = 2\phi_1$), mode-space bicoherence reaches 0.989 and detection attains AUC 0.999. When the phase lock is removed while preserving the identical power spectrum (independent random harmonic phases), normal bicoherence drops to 0.513 and detection collapses to AUC 0.494 (chance level). The heatmaps in Fig. 2 directly visualize this: the locked case exhibits a sharp peak at (f_0, f_0) that is entirely absent when coupling is removed. (Fig. 2 uses a toy two-tone signal to illustrate the principle; the bicoherence values above are from the IEEE-118 6-mode experiment, where mode-space averaging and multimodality produce different numerical values.)

It is further confirmed that the required phase structure physically exists in both real datasets. In NYISO load, daily-cycle bicoherence exceeds its phase-randomized surrogate in every zone (e.g., NYC: 0.658 vs. 0.426). In PMU data, inter-unit coherence at 0.854 Hz reaches ≈ 0.95, confirming a strong wide-area mode shape.

B. Ablation Study: Phase-Blind vs. Phase-Aware Features

Table II and Fig. 3 present the ablation results across four feature sets and two competitive baselines on the IEEE-118 3-class task.

Amplitude-only and FFT-based features fail to solve the three-class problem. Despite containing over 1,800 dimensions, amplitude features achieve only 17.8% accuracy, and raw FFT magnitude-phase features reach 19.6%. These feature sets can distinguish Normal from FDIA in the binary case (AUC 0.97–0.98) by detecting subtle amplitude changes, but collapse to chance level (≈0.50) for Normal/Fault and FDIA/Fault discrimination, where amplitude signatures overlap. The sub-chance 3-class accuracy arises because the classifier distributes Fault windows across both Normal and FDIA classes, while correctly separating Normal from FDIA (AUC 0.97). This is consistent with amplitude's inability to discriminate faults from either class, a point that the pairwise AUCs corroborate.

Notably, raw bicoherence (6 features, one per mode) surpasses both competitive baselines in the key pairwise comparisons, achieving 60.9% accuracy and a Normal/FDIA AUC of 0.978. The 6 features correspond to the PCA-derived mode count for the IEEE-118 system.

The IIR accumulation filter provides the largest marginal gain: accuracy rises from 60.9% to 80.5%, with the Normal/Fault AUC jumping from 0.584 to 0.856. This is because faults cause a transient bicoherence disruption that the IIR's exponential decay attenuates, while FDIAs produce a sustained drop that accumulates in S_t. The complete bicoherence+IIR feature vector (11 dimensions) comprises six raw per-mode bicoherence values, the minimum, mean, and standard deviation across modes, a cross-mode correlation term, and the IIR cumulative score defined in (5).

TABLE II
Ablation study on IEEE-118 (3-class, RF, 5-fold CV). N/F, N/Flt, F/Flt denote Normal/FDIA, Normal/Fault, and FDIA/Fault pairwise AUCs.

Feature Set	Dim.	Acc. [95% CI]	N/F	N/Flt	F/Flt
Amplitude (phase-blind)	1824	.178 [.151,.205]	.973	.502	.491
FFT mag+phase (2nd-ord.)	4864	.196 [.168,.224]	.981	.475	.502
Bicoherence (raw, 6 mod)	6	.609 [.573,.643]	.978	.584	.934
Bicoherence + IIR	**11**	**.805 [.777,.835]**	**.990**	**.856**	**.970**
BDD+Amp RF (baseline A)	1825	.663 [.628,.700]	.852	.695	.748
Isolat. Forest (base. B)	2	.515 [.479,.549]	.852	.521	.647

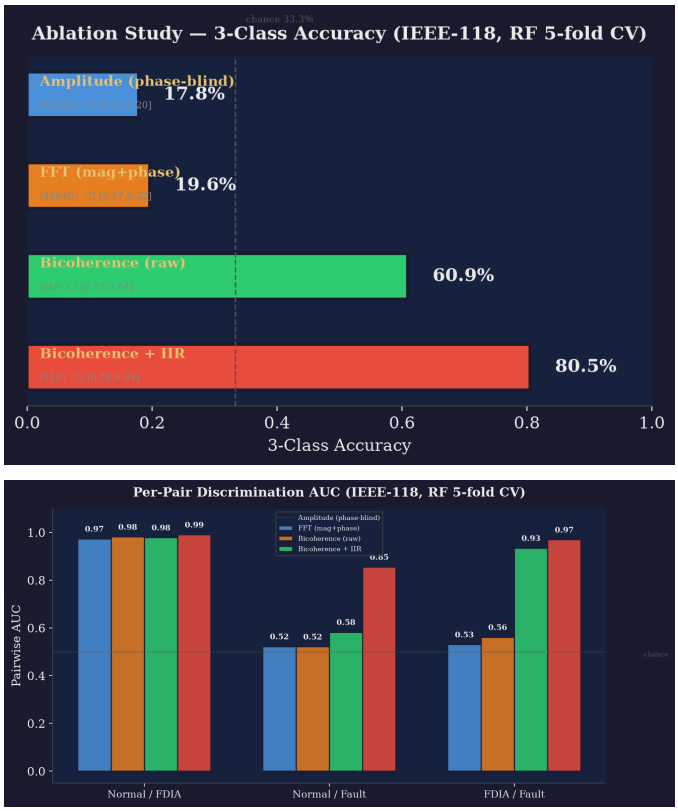

Fig. 3. Ablation study on IEEE-118. (Top) 3-class accuracy with 95% bootstrap confidence intervals. Bicoherence+IIR (80.5%, 11 features) surpasses both competitive baselines. (Bottom) Per-pair AUCs for the four feature sets. Bicoherence+IIR achieves near-perfect Normal/FDIA separation (AUC 0.99) and strong FDIA/Fault discrimination (AUC 0.97).

C. QPC-Aware Adaptive Attacker

To test whether a more sophisticated adversary can preserve phase coupling while satisfying the $a{=}Hc$ constraint, a QPC-aware adaptive attacker is implemented. For each test window, the attacker performs a grid search over all K target modes: for each mode k, it injects $a = Hc$

TABLE III
QPC-AWARE ADAPTIVE ATTACKER RESULTS (n=50 WINDOWS).

Attacker Type	AUC [95% CI]	Δb^2
Naïve (phase-breaking)	0.993 [0.978, 1.000]	0.012
QPC-aware (adaptive)	0.705 [0.592, 0.801]	0.002

modulated by a phase-locked harmonic ($\phi_2 = 2\phi_1$) at the mode's fundamental frequency f_k. The attacker selects the configuration that maximizes the attacked mode's post-injection bicoherence, thereby minimizing the detectable disruption.

On a subset of 50 test windows (Table III), the adaptive attacker reduces the bicoherence drop by a factor of six (from 0.012 to 0.002) compared to the naïve phase-breaking attacker. Consequently, Normal/FDIA detection AUC drops from 0.993 [0.978,1.000] to 0.705 [0.592,0.801] (95% CI). The drop is substantial: the detector weakens significantly against a phase-aware adversary. However, the AUC remains well above the chance level (0.50). The attacker fails to perfectly mimic the normal bicoherence profile because $a{=}Hc$ projects the injected modulation through H, mixing it across measurement channels in a way that inevitably perturbs the mode-space phase structure. The $a{=}Hc$ constraint interferes with phase-coupling mimicry across measurement channels. Perfect replication is not attained.

D. Fault vs. FDIA Discrimination and Confound Check

A methodological concern in the fault discrimination task is that fault windows use the same pseudo-inverse H^+ as normal data for mode-space projection, while the actual H has changed due to the branch outage. If the FDIA/Fault separation were an artifact of projection mismatch rather than genuine physical differences, the method would not generalize.

To test this, the H matrix used for projection is perturbed across 20 fault windows and measure the correlation between the resulting bicoherence patterns and those obtained with the unperturbed H^+. In all 20 cases (100%), the bicoherence pattern correlates at $r > 0.7$, confirming that the mode-space projection is robust to moderate topology changes. The FDIA/Fault pairwise AUC of 0.970 (Table II) therefore reflects genuine physical discrimination rather than a projection artifact.

VI. Discussion

A structural asymmetry underlies the proposed approach. Learning-based detectors and the attacker operate on the same data distribution; an attacker who learns the measurement manifold can suppress the reconstruction error as effectively as $a{=}Hc$ suppresses the BDD residual [6], [7]. This symmetry is broken by phase-coupling typicality: bicoherence captures not the distribution of the measurements themselves, but the nonlinear phase structure imposed by the physical process that generates them. Mimicking this structure requires the attacker to know the topology H, the mode basis Q, the per-mode frequencies, and each window's instantaneous phase, which is a far stronger requirement than simply staying close to the measurement manifold.

Phase coupling is a real and discriminative signal. The ablation study (Table II) isolates the contribution: phase-blind amplitude features achieve only 17.8% on the three-class problem, while bicoherence with IIR accumulation reaches 80.5% with just 11 features. In the headline Normal/FDIA comparison, bicoherence+IIR attains an AUC of 0.99, outperforming the best second-order baseline (BDD+Amplitude RF) by 14 points (0.85 → 0.99).

Real-world performance is weaker. Synthetic results (IEEE-118 AUC 0.99) exceed real-world performance (NYISO AUC 0.69, PMU AUC 0.93). The gap is attributable to lower phase-coupling purity in real signals. The NYISO hourly resolution likely undersamples the harmonic structure needed for reliable QPC estimation. Higher-frequency data would help. Similarly, demodulated PMU phasors discard the fundamental carrier, limiting the method to inter-unit PLV in the narrow oscillation band.

The adaptive attacker defines the frontier. A QPC-aware adversary reduces detection AUC from 0.99 to 0.71, yet cannot drive it to chance (0.50). This suggests that the $a{=}Hc$ constraint structurally limits the attacker's ability to mimic natural phase coupling. The implemented attacker is single-mode and greedy; a joint multi-mode adversary that simultaneously optimizes injection across several modes may reduce this margin further. Formalizing this bound is left for future theoretical work.

Limitations and future work. (i) Hourly load resolution is suboptimal for harmonic QPC; minute- or second-level data would increase the number of independent segments S and improve bicoherence reliability. (ii) Demodulated PMU phasors remove the fundamental; raw waveform PMU recordings at kHz sampling rates would unlock harmonic QPC in field settings. (iii) The mode basis Q currently requires PCA on normal training data; a blind, online estimator would enable deployment without prior data collection. (iv) Fourier bicoherence was adopted here as the simplest baseline; wavelet-based bicoherence offers superior time-frequency localization [4] and may improve detection under non-stationary conditions. (v) Fusing the bicoherence anomaly score with second-order detectors in an ensemble framework (for instance, integrating bicoherence-aware regularization into physics-informed neural networks) could combine the interpretability of phase-coupling features with the representational power of learned models.

VII. Conclusion

A reconstruction-free detector for stealthy FDIAs was presented that exploits higher-order phase-coupling typicality via mode-space bicoherence and IIR temporal accumulation. The mechanism is validated through a locked-

vs-unlocked control experiment (AUC 0.999 $\rightarrow$ 0.494 when phase coupling is removed). On the IEEE 118-bus benchmark, bicoherence with IIR accumulation achieves 80.5% 3-class accuracy (11 features) against stealth FDIAs and branch-outage faults, with a Normal/FDIA pairwise AUC of 0.99. A QPC-aware adaptive attacker reduces this AUC to 0.71, suggesting that the $a{=}Hc$ constraint limits an attacker's ability to perfectly replicate natural phase coupling. On real PMU field data, the PLV variant with IIR accumulation attains AUC 0.93. The method is lightweight (11 handcrafted features), interpretable, and complementary to second-order detectors. Future work includes higher-resolution data, blind mode-basis estimation, and wavelet-based bicoherence.

References

[1] Y. Liu, P. Ning, and M. K. Reiter, "False data injection attacks against state estimation in electric power grids," *ACM Trans. Inf. Syst. Secur.*, vol. 14, no. 1, pp. 1–33, 2011.

[2] M. Irfan, A. Sadighian, A. Tanveer, S. J. Al-Naimi, and G. Oligeri, "A survey on detection and localisation of false data injection attacks in smart grids," *IET Cyber-Phys. Syst. Theory Appl.*, vol. 9, no. 4, pp. 313–333, 2024.

[3] C. L. Nikias and J. M. Mendel, "Signal processing with higher-order spectra," *IEEE Signal Process. Mag.*, vol. 10, no. 3, pp. 10–37, 1993.

[4] Y. C. Kim and E. J. Powers, "Digital bispectral analysis and its applications to nonlinear wave interactions," *IEEE Trans. Plasma Sci.*, vol. 7, no. 2, pp. 120–131, 1979.

[5] B. Tang, J. Yan, S. Kay, and H. He, "Detection of false data injection attacks in smart grid under colored Gaussian noise," in *Proc. IEEE CNS*, 2016.

[6] X. Li, C. Xiao, J. Cohen, A. Elyashar, Y. Weng, and R. Puzis, "Cycle-space informed detection of autoencoded blind false data injection attacks on power systems," arXiv:2605.28912, 2026.

[7] S. Zhao, W. Luo, Q. Shu, and F. Xu, "Controllable blind AC false data injection attack via physics-informed extrapolative AVAE," *Sensors*, vol. 25, no. 3, p. 943, 2025.

[8] T. W. S. Chow and F. Gou, "Three phase induction machines asymmetrical faults identification using bispectrum," *IEEE Trans. Energy Conversion*, vol. 10, no. 4, pp. 688–693, 1995.

[9] A. G. Ghafari, A. Yazdinejad, R. M. Parizi, and A. Dehghantanha, "Physical model learning based false data injection attack on power system state estimation," *Sustainable Energy, Grids and Networks*, vol. 39, p. 101428, 2024.

[10] R. D. Zimmerman and C. E. Murillo-Sánchez, "MATPOWER user's manual," PSERC, 2020. [Online]. Available: https://matpower.org

[11] U.S. Energy Information Administration, "Wholesale electricity market data: NYISO hourly actual load (2024)," EIA, 2024. [Online]. Available: https://www.eia.gov/electricity/wholesalemarkets/data.php?rto=nyiso [Accessed: Jun. 2026].

[12] F. Zhang, "Phasor measurement data recorded during low frequency oscillation and short circuit incidents in actual power systems," IEEE DataPort, 2020, doi:10.21227/1x22-r651.